

# Semi-parametric bulk and tail regression using spline-based neural networks

Reetam Majumder

Department of Mathematical Sciences

University of Arkansas

and

Jordan Richards

School of Mathematics and Maxwell Institute for Mathematical Sciences

University of Edinburgh

April 29, 2025

## Abstract

Semi-parametric quantile regression (SPQR) is a flexible approach to density regression that learns a spline-based representation of conditional density functions using neural networks. As it makes no parametric assumptions about the underlying density, SPQR performs well for in-sample testing and interpolation. However, it can perform poorly when modelling heavy-tailed data or when asked to extrapolate beyond the range of observations, as it fails to satisfy any of the asymptotic guarantees provided by extreme value theory (EVT). To build semi-parametric density regression models that can be used for reliable tail extrapolation, we create the blended generalised Pareto (GP) distribution, which i) provides a model for the entire range of data and, via a smooth and continuous transition, ii) benefits from exact GP upper-tails without the need for intermediate threshold selection. We combine SPQR with our blended GP to create extremal semi-parametric quantile regression (xSPQR), which provides a flexible semi-parametric approach to density regression that is compliant with traditional EVT. We handle interpretability of xSPQR through the use of model-agnostic variable importance scores, which provide the relative importance of a covariate for separately determining the bulk and tail of the conditional density. The efficacy of xSPQR is illustrated on simulated data, and an application to U.S. wildfire burnt areas.

*Keywords:* blended generalised Pareto distribution, conditional density estimation, deep extreme quantile regression, explainable AI, extreme value theory

# 1 Introduction

Extreme quantile regression models provide a useful tool for risk assessment in a wide range of applied fields, such as econometrics (Chavez-Demoulin and Guillou, 2018; Daouia et al., 2019, 2023), insurance (Daouia et al., 2024), natural hazard modelling (Richards and Huser, 2022; Yadav et al., 2023), chemometrics (Gardes and Stupler, 2019), flood risk assessment (Jóhannesson et al., 2022; Pasche and Engelke, 2024), and downscaling (Wang et al., 2012). A common approach to extreme quantile regression follows via a parametric assumption on the upper-tails of the conditional distribution of a response variable  $Y \in \mathbb{R}$  given a set of realised covariates  $\mathbf{x} \in \mathbb{R}^p$  of a random vector  $\mathbf{X}$ . The de-facto standard assumption is that excesses of  $Y$  above a high threshold  $u(\mathbf{x})$  follow a generalised Pareto (GP) distribution (see, e.g., Coles (2001) for discussion) with covariate-dependent shape and scale parameters,  $\xi(\mathbf{x}) \in \mathbb{R}$  and  $\sigma_u(\mathbf{x}) > 0$ , respectively; that is, one assumes the parametric GP regression model:

$$(Y - u(\mathbf{x})) \mid (Y > u(\mathbf{x}), \mathbf{X} = \mathbf{x}) \sim \text{GP}(\sigma_u(\mathbf{x}), \xi(\mathbf{x})),$$

where the scale  $\sigma_u(\mathbf{x})$  is dependent on the threshold  $u(\mathbf{x})$ . A regression model of this form benefits from the asymptotic guarantees of the GP distribution (e.g., threshold stability; see Coles, 2001), and allows for reliable estimation of extreme conditional  $\tau$ -quantiles (for  $\tau \in (0, 1)$  close to one); see Davison and Smith (1990) for details.

The choice of the intermediate threshold  $u(\mathbf{x})$  is an ubiquitous problem in extreme value theory (EVT) (see, e.g., Murphy et al., 2024). In a regression setting, the threshold  $u(\mathbf{x})$  can be modelled as a function of covariates; choosing and estimating an appropriate model for  $u(\mathbf{x})$  introduces uncertainty into the modelling procedure. Moreover, the additional complication that the scale  $\sigma_u(\mathbf{x})$  depends on  $u(\mathbf{x})$  makes interpretability of model estimates difficult (Richards et al., 2023). To overcome the problem of threshold choice, one can

replace the parametric GP model (for threshold excesses) with a model for the entire support of data that retains (exact or approximate) GP upper-tails, without requiring threshold estimation. Many such univariate models have been proposed in the literature (see review by Scarrott and MacDonald, 2012). Examples include splicing or mixing of density functions (with at least one constituent density being the GP density; see, e.g., Frigessi et al., 2002; Behrens et al., 2004; de Melo Mendes and Lopes, 2004; Carreau and Bengio, 2007; Reynkens et al., 2017; Castro-Camilo et al., 2019), blending of distribution functions (Castro-Camilo et al., 2022; Krakauer, 2024), or parametric generalisations of the GP distribution (Papastathopoulos and Tawn, 2013; Naveau et al., 2016; Stein, 2021a,b). Although these all-in-one models are compliant with traditional EVT, and can thus perform reliable extrapolation into the upper-tail, they often suffer in terms of flexibility as both the bulk and tail of the distribution are parametric. Bulk and tail models with non-parametric bodies have been proposed (e.g., Tancredi et al., 2006; MacDonald et al., 2011; Tencaliec et al., 2020), but these are yet to be extended to the regression setting.

After estimating  $u(\mathbf{x})$ , a further modelling choice for GP regression is the functional forms of  $\sigma_u(\mathbf{x})$  and  $\xi(\mathbf{x})$ . Although classical GP regression models used linear models (e.g., Davison and Smith, 1990; Wang et al., 2012), there has been growing interest in more flexible and computationally-scalable alternatives, including additive models (Chavez-Demoulin and Davison, 2005; Youngman, 2019), local kernel smoothing (Daouia et al., 2011; Velthoen et al., 2019; Gardes and Stupler, 2019), decision trees (Farkas et al., 2021, 2024), random forests (Gnecco et al., 2024), gradient boosting (Koh, 2023; Velthoen et al., 2023), and deep neural networks (Wilson et al., 2022; Richards et al., 2023; Cisneros et al., 2024; Pasche and Engelke, 2024; Mackay et al., 2024). In particular, deep parametric GP regression methods (i.e., those that exploit neural networks for modelling  $\sigma_u(\mathbf{x})$  and

$\xi(\mathbf{x})$ ; see overview by Richards and Huser, 2024) are particularly appealing as they are highly flexible, scalable to high covariate dimension  $p$ , and can be estimated quickly using easily-accessible software packages (see, e.g., Richards, 2022). However, existing deep GP regression models suffer from the same two limitations of all parametric GP regression models: i) they require modelling and estimation of the intermediate threshold  $u(\mathbf{x})$ , and ii) they do not provide a model for the bulk (or body) and lower-tails of the conditional distribution, that is,  $Y \mid (Y < u(\mathbf{x}), \mathbf{X} = \mathbf{x})$ .

To create flexible, semi-parametric regression models that are EVT-compliant and capable of modelling the entire range of the response data, we introduce the blended GP (bGP) distribution. Similarly to the construction of the blended generalised extreme value distribution of Castro-Camilo et al. (2022), we blend the GP distribution with an appropriately chosen distributional model for the bulk of the data. The bGP distribution can model the entire range of data, and has exact GP upper-tails without the need for threshold selection. We utilise the blended GP for regression by combining a deep GP regression model, for the upper-tails, with a deep semi-parametric regression model for the bulk of the distribution. For the latter, we employ the semi-parametric quantile regression (SPQR) model of Xu and Reich (2021), which has been used previously for inference with spatial extremal processes (Majumder and Reich, 2023; Majumder et al., 2024b). Via a spline-based representation of conditional densities, the SPQR framework provides a flexible description of the conditional bulk without any parametric assumptions. While it has been shown to work extremely well for in-sample prediction, the SPQR model assumes finite support for the response variable  $Y$ , and so cannot be readily used to perform extrapolation beyond the range of the observations. However, in conjunction with a blended GP regression model, we create a very flexible density regression model that is EVT-compliant; we refer to this

framework as extremal semi-parametric quantile regression (xSPQR).

The contributions of this work are threefold: i) we introduce the (unconditional) blended GP (bGP) distribution, which provides a new univariate distribution that can jointly model the bulk and upper-tail of data; ii) we develop the xSPQR framework for all-in-one, EVT-compliant density regression and extrapolation; and iii) we showcase interpretability of the xSPQR method through the use of accumulative local effects (ALEs; Apley and Zhu, 2020), which are a model-agnostic metric for assessing relative variable importance.

The rest of this paper is organised as follows. In Section 2, we provide the background on SPQR. In Section 3, we introduce the blended GP distribution, and combine this with SPQR to create xSPQR, with details on estimation of variable importance provided in Section 3.5. In Section 4, we conduct simulation studies to demonstrate the efficacy of xSPQR and its ability to capture covariate effects on both the bulk and tails of the conditional density function. In Section 5, we apply xSPQR to model the entire range of burnt areas from moderate and extreme wildfire in the contiguous United States (U.S.) between 1990–2020. We conclude in Section 6 with a discussion, and outline avenues for further research.

## 2 Background

### 2.1 Overview

In Section 2.2, we provide the background details on the semi-parametric quantile regression (SPQR) framework. In Section 2.3, we describe accumulated local effects (ALEs) for assessing relative variable importance with SPQR.

## 2.2 Semi-parametric quantile regression

Semi-parametric quantile regression (SPQR) was introduced by Xu and Reich (2021) as an approach to conditional density estimation which makes no parametric assumptions about the underlying distribution. Consider a response variable  $Y \in [0, 1]$  and a set of realised covariates  $\mathbf{x} \in \mathcal{X}$  of a random vector  $\mathbf{X}$ , where  $\mathcal{X} \subset \mathbb{R}^p$  denotes the sample space of  $\mathbf{X}$ . Then, SPQR assumes that the conditional density of  $Y | \mathbf{X} = \mathbf{x}$  is a function of  $K$  third-order  $M$ -spline basis functions,  $\{M_1(y), \dots, M_K(y)\}$ , with  $K + 2$  knots spanning the unit interval  $[0, 1]$ .  $M$ -spline basis functions are supported on a compact interval, positive, and integrate to one, giving them a natural interpretation as density functions. Moreover, both the  $M$ -spline basis function and its integral, the  $I$ -spline basis function, have a closed-form construction, which permits efficient inference and prediction with SPQR; see Appendix A for details. We further note that a convex combination of  $M$ -spline ( $I$ -spline) basis functions is a valid density (distribution) function supported on a compact interval (Ramsay, 1988). The SPQR model assumes that the conditional density can be represented as a convex combination of  $M$ -spline basis functions:

$$f_{\text{SPQR}}(y|\mathbf{x}) = \sum_{k=1}^K w_k(\mathbf{x}) M_k(y), \quad (1)$$

with weights  $w_k(\mathbf{x}) : \mathcal{X} \mapsto [0, 1]$ ,  $k = 1, \dots, K$ , satisfying  $\sum_{k=1}^K w_k(\mathbf{x}) = 1$  for all  $\mathbf{x} \in \mathcal{X}$ .

By increasing the number  $K$  of basis functions and appropriately selecting the weights, the mixture density in (1) can approximate any continuous density function (Chui et al., 1980; Abrahamowicz et al., 1992). To model the weights in a flexible manner, Xu and Reich (2021) use a multi-layer perceptron (MLP), a type of neural network. The MLP has  $H$  hidden layers with non-linear activation functions; common activation functions used in previous applications of SPQR include the sigmoid and rectified linear unit (ReLU, Nair and Hinton, 2010) functions, which we consider in this work. The additional final layer

of the MLP outputs the weights  $\{w_k\}_{k=1}^K$  and has a softmax activation function, which ensures that the outputs sum to one. The width of each hidden layer is determined by the number of nodes,  $n_h \in \mathbb{N}$ , for  $h = 1, \dots, H$ .

The MLP is constructed via a system of recursive equations: the output of the  $h$ -th layer,  $\mathbf{x}^{(h)}$ , is

$$\begin{aligned} \mathbf{x}^{(h)} &:= \phi(\mathbf{W}^{(h)}\mathbf{x}^{(h-1)} + \mathbf{b}^{(h)}), \quad h = 1, \dots, H, \\ \mathcal{W}(\mathbf{x}) &:= \mathbf{x}^{(H+1)} = \text{softmax}(\mathbf{W}^{(H+1)}\mathbf{x}^{(H)} + \mathbf{b}^{(H+1)}), \end{aligned} \quad (2)$$

where  $\phi$  is the non-linear activation function,  $\mathbf{x}^{(0)} := \mathbf{x}$  corresponds to the input covariates, and  $\mathcal{W}(\mathbf{x}) = \{w_k(\mathbf{x})\}_{k=1}^K$  is a  $K$ -vector of weights satisfying  $\sum_{k=1}^K w_k(\mathbf{x}) = 1$  for all  $\mathbf{x} \in \mathcal{X}$ . The estimable ‘‘weights’’ and ‘‘biases’’ of the MLP are contained in  $\boldsymbol{\theta} := \{\mathbf{W}^{(h)}, \mathbf{b}^{(h)}\}_{h=1}^{H+1}$ , where  $\mathbf{W}^{(h)} \in \mathbb{R}^{n_h \times n_{h-1}}$  and  $\mathbf{b}^{(h)} \in \mathbb{R}^{n_h}$  are layer-specific weight matrices and bias vectors, respectively, with input dimension  $n_0 := p$ . Note that the dependence of  $\mathcal{W}(\cdot)$  (and its elements) on  $\boldsymbol{\theta}$  has been omitted from notation for simplicity. If each layer is represented by a function, say  $f^{(h)}(\cdot)$  (suppressing the dependence on  $\boldsymbol{\theta}$  and  $\mathbf{X}$  for convenience), the MLP  $f : \mathbb{R}^q \rightarrow \mathbb{R}^K$  is a composition of the layer operations, i.e.,  $f(\cdot) := f^{(H+1)} \circ \dots \circ f^{(1)}(\cdot)$ .

We use stochastic gradient descent and the adaptive moment estimation (Adam) optimizer (Kingma and Ba, 2014) to optimise  $\boldsymbol{\theta}$ . The optimised loss function is the negative log-likelihood associated with (1). Hyper-parameters, such as the number of hidden layers  $H$ , the dimension  $n_h$  of each hidden layer, the activation function  $\phi$ , and the number of basis functions  $K$ , are tuned using a grid search. Computing the conditional density function (1) is simple and fast given the parameters  $\boldsymbol{\theta}$ . Additionally, the expression for the distribution function is also available in closed form:

$$F_{\text{SPQR}}(y|\mathbf{x}) = \sum_{k=1}^K w_k(\mathbf{x}) I_k(\mathbf{x}), \quad (3)$$

where  $\{I_k(\cdot)\}_{k=1}^K$  are  $I$ -spline basis functions; note that the weights  $\{w_k(\mathbf{x})\}_{k=1}^K$  do not differ between the density and distribution function in (1) and (3), respectively. Finally, the conditional quantile function for level  $\tau \in (0, 1)$  is defined as  $Q_{\text{SPQR}}(\tau|\mathbf{x})$ , such that

$$F_{\text{SPQR}}\{Q_{\text{SPQR}}(\tau|\mathbf{x})|\mathbf{x}\} = \tau.$$

While  $Q_{\text{SPQR}}(\tau|\mathbf{x})$  is not available in closed-form (unlike  $f_{\text{SPQR}}(y|\mathbf{x})$  and  $F_{\text{SPQR}}(y|\mathbf{x})$ ) it can be quickly approximated using interpolation. Finally, we note that SPQR can accommodate the special case where  $\mathbf{X}$  is just an intercept term, which is equivalent to unconditional density estimation; this has been recently explored by Majumder et al. (2024a).

### 2.3 Assessing relative variable importance for SPQR

The SPQR framework quantifies the effect of the covariates on specific levels of the response distribution via the quantile function  $Q_{\text{SPQR}}(\tau|\mathbf{x})$ , where  $\tau \in (0, 1)$  is the quantile level of interest. In previous work using SPQR (see e.g., Majumder et al., 2024b; Majumder and Reich, 2023), covariate effects on  $\tau$ -quantiles have been measured using accumulative local effects (ALEs; Apley and Zhu, 2020). We briefly outline ALEs and their link to relative variable importance quantification; we consider the effects of covariates on a generic differentiable function  $g(\mathbf{x})$ , where  $\mathbf{x} = (x_1, \dots, x_p)$  is the vector of covariates. The sensitivity of  $g(\mathbf{x})$  to covariate  $x_j$  is quantified by the partial derivative

$$\dot{g}_j(x_j) = \frac{\partial g(\mathbf{x})}{\partial x_j}.$$

The accumulated local effect (ALE) of  $x_j$  on  $g(\cdot)$  is then defined as

$$\text{ALE}_j(x_j; g) = \int_{z_{0,j}}^{x_j} \mathbb{E}[\dot{g}_j(x_j)|x_j = z_j] dz_j,$$

where  $z_{0,j}$  is an approximate lower bound for  $x_j$ . In practice,  $\text{ALE}_j(x_j; g)$  is estimated by replacing the above integral with a partial sum, which can be used even when  $g(\mathbf{x})$  is

not differentiable. The  $\text{ALE}_j(x_j; g)$  scores provides the relative importance of a specific value of the  $j$ -th covariate,  $x_j$ , on the function  $g(\cdot)$ . Following Greenwell et al. (2018), we can measure the heterogeneity of the effect of covariate  $X_j$  on  $g(\cdot)$  by taking the standard deviation of  $\text{ALE}_j(X_j; g)$  with respect to the distribution of  $X_j$ . We thus define the variable importance (VI) scores for  $X_j$  on  $g(\cdot)$  by

$$\text{VI}_j(g) = \sqrt{\text{Var}_{X_j}[\text{ALE}_j(X_j; g)]}.$$

This is estimated empirically using observed samples of  $X_j$ . For SPQR, where  $g(\cdot)$  corresponds to the conditional  $\tau$ -th quantile function, we typically estimate  $\text{VI}_j(g)$  for a sequence of  $\tau$  values and for all  $j = 1, \dots, p$ .

### 3 Extremal semi-parametric quantile regression

#### 3.1 Overview

In Section 3.2, we present the blended generalised Pareto distribution. In Section 3.3, we describe the extremal semi-parametric quantile regression (xSPQR) framework, which blends the SPQR representation for conditional densities with a deep GP regression model (as discussed in Section 1). Section 3.4 details inference for xSPQR, and Section 3.5 describes estimation of relative variable importance for the conditional upper-tails.

#### 3.2 Blended generalised Pareto distribution

Castro-Camilo et al. (2022) introduced the blended generalised extreme value distribution (bGEV), which combines the lower (exponential) tail of a Gumbel distribution with the upper (heavy) tail of a Fréchet distribution; Krakauer (2024) extended the blended GEV to allow for bounded or light-tailed margins. The blended GEV has already been shown to be

an effective model for deep extreme quantile regression; see, e.g., Richards and Huser (2022) and Richards and Huser (2024). We follow a similar approach to Castro-Camilo et al. (2022) and construct the blended GP distribution (bGP), which blends together a constituent “bulk” distribution, describing the body, with the GP distribution, for the upper-tails. We present here the bGP for an arbitrary bulk distribution, in the unconditional setting, i.e., we consider a continuous random variable  $Y \geq 0$ , but no covariate information. We discuss the conditional setting as a natural extension towards EVT-compliant density regression in Section 3.3, where we take the bulk distribution to be the SPQR representation of conditional densities, as defined in (3). This creates a conditional distribution function that exhibits great flexibility in the body, while retaining the exact GP upper-tails of standard parametric extreme quantile regression models.

Let  $F(y|\mathcal{W})$ ,  $f(y|\mathcal{W})$ , and  $Q(y|\mathcal{W})$  denote the distribution, density, and quantile functions, respectively, of a continuous random variable, which have estimable parameters contained in  $\mathcal{W}$ ; here  $F(y|\mathcal{W})$  and  $f(y|\mathcal{W})$  are supported on the interval  $[0, 1]$  and referred to as the “bulk” distribution and density, respectively. We then let  $F_{\text{GP}}(y|u, \sigma_u, \xi)$ ,  $f_{\text{GP}}(y|u, \sigma_u, \xi)$ , and  $Q_{\text{GP}}(y|u, \sigma_u, \xi)$  denote the distribution, density, and quantile functions, respectively, of a generalised Pareto random variable with scale parameter  $\sigma_u > 0$ , shape parameter  $\xi \in \mathbb{R}$ , and threshold  $u \in \mathbb{R}$ . The distribution function  $F_{\text{GP}}(y|u, \sigma_u, \xi)$  is

$$F_{\text{GP}}(y|u, \sigma_u, \xi) := \begin{cases} 1 - (1 + \xi(y - u)/\sigma_u)^{-1/\xi}, & \xi \neq 0, \\ 1 - \exp(-(y - u)/\sigma_u), & \xi = 0; \end{cases}$$

note that, unlike the aforementioned distribution for the bulk,  $F_{\text{GP}}(y|u, \sigma_u, \xi)$  is supported on  $y \geq u$  if  $\xi \geq 0$  and, otherwise,  $y \in [u, u - \sigma_u/\xi]$ .

We define the blended GP distribution, denoted by  $\text{bGP}(\mathcal{W}, \xi)$ , via its continuous dis-

tribution function  $H(y|\mathcal{W}, \xi)$ , defined as

$$H(y|\mathcal{W}, \xi) = \begin{cases} F(y|\mathcal{W})^{1-p(y)} F_{\text{GP}}(y|\tilde{u}, \tilde{\sigma}_u, \xi)^{p(y)}, & y > \tilde{u}, \\ F(y|\mathcal{W}), & y \leq \tilde{u}, \end{cases} \quad (4)$$

where  $p(y) \in [0, 1]$  is a weighting function. The distribution function  $H(y|\mathcal{W}, \xi)$  inherits support from the constituent distribution functions; the lower bound of the support is zero, whilst the upper bound is infinite if  $\xi \geq 0$  and  $\tilde{u} - \tilde{\sigma}_u/\xi > 0$ , otherwise. Following Castro-Camilo et al. (2022), we take the weighting function to be

$$p(y) = p(y; a, b, c_1, c_2) = F_{\text{Beta}}\left(\frac{y-a}{b-a}, c_1, c_2\right),$$

where  $F_{\text{Beta}}(\cdot, c_1, c_2)$  denotes the distribution function of a  $\text{Beta}(c_1, c_2)$  random variable with shape parameters  $c_1 > 0$  and  $c_2 > 0$ . We blend the density functions  $F(\cdot|\mathcal{W})$  and  $F_{\text{GP}}(\cdot|u, \sigma_u, \xi)$  within the interval  $[a, b]$ , where the bounds are taken to be the  $p_a$  and  $p_b$  quantiles of  $F(\cdot)$ . That is, for  $p_a, p_b \in (0, 1)$  with  $p_a < p_b$ , we take  $a := Q(p_a|\mathcal{W})$  and  $b := Q(p_b|\mathcal{W})$ . To ensure continuity of  $H(\cdot|\mathcal{W}, \xi)$ , we require  $F(a|\mathcal{W}) = F_{\text{GP}}(a|\tilde{u}, \tilde{\sigma}_u, \xi)$  and  $F(b|\mathcal{W}) = F_{\text{GP}}(b|\tilde{u}, \tilde{\sigma}_u, \xi)$ ; this is achieved by setting

$$(\tilde{\sigma}_u, \tilde{u}) = \begin{cases} \left(\frac{\xi(a-b)}{(1-p_a)^{-\xi} - (1-p_b)^{-\xi}}, a - \frac{(a-b)\{(1-p_a)^{-\xi} - 1\}}{(1-p_a)^{-\xi} - (1-p_b)^{-\xi}}\right), & \xi \neq 0, \\ \left(\frac{(a-b)}{\log(1-p_b) - \log(1-p_a)}, a - \frac{(a-b)\{-\log(1-p_a)\}}{\log(1-p_b) - \log(1-p_a)}\right), & \xi = 0. \end{cases} \quad (5)$$

Note that  $\tilde{u} < a$  and, for  $\xi < 0$ , the upper-endpoint of  $H(\cdot|\mathcal{W}, \xi)$  satisfies  $\tilde{u} - \tilde{\sigma}_u/\xi > b$ ; given also that  $p(y) = 0$  for any  $y < a$ , it follows that  $H(\cdot|\mathcal{W}, \xi)$  is continuous. The bGP distribution has two estimable parameters,  $\mathcal{W}$  and  $\xi$ , which respectively determine the bulk and upper-tail. The GP threshold  $u$  and scale parameter  $\sigma_u$  are deterministic functions of  $\mathcal{W}$  and  $\xi$ . It is clear to see that, for large  $y > \tilde{u}$ ,  $H(\cdot|\mathcal{W}, \xi)$  is exactly the GP distribution function, with a freely-varying tail index  $\xi$  that is not determined by parameters  $\mathcal{W}$  for the bulk distribution.

The density function of a  $\text{bGP}(\mathcal{W}, \xi)$  random variable has the closed-form expression

$$h(y|\mathcal{W}, \xi) = H(y|\mathcal{W}, \xi) \times \left\{ p'(y) \log F_{\text{GP}}(y|\tilde{u}, \tilde{\sigma}_u, \xi) + p(y) \frac{f_{\text{GP}}(y|\tilde{u}, \tilde{\sigma}_u, \xi)}{F_{\text{GP}}(y|\tilde{u}, \tilde{\sigma}_u, \xi)} \right. \\ \left. - p'(y) \log F(y|\mathcal{W}) + (1 - p(y)) \frac{f(y|\mathcal{W})}{F(y|\mathcal{W})} \right\}, \quad (6)$$

where  $p'(y) = (b - a)^{-1} f_{\text{Beta}}\left(\frac{y-a}{b-a}, c_1, c_2\right)$  for  $f_{\text{Beta}}(\cdot, c_1, c_2)$  the density of the Beta distribution with shape parameters  $c_1$  and  $c_2$ . As discussed by Castro-Camilo et al. (2022), setting  $c_1, c_2 > 3$  ensures that the second derivative of the log-density is always continuous; we hereafter assume this to hold.

### 3.3 Tail density regression using xSPQR

We now describe the extremal semi-parametric quantile regression framework, xSPQR. Remaining in the unconditional setting, we first create a flexible bGP distribution by constructing the constituent bulk distribution and density functions,  $F(y|\mathcal{W})$  and  $f(y|\mathcal{W})$ , respectively, in (4), via the usual SPQR representation, i.e., we set  $F(y|\mathcal{W}) = F_{\text{SPQR}}(y|\mathcal{W})$  (and  $f(y|\mathcal{W}) = f_{\text{SPQR}}(y|\mathcal{W})$ ), which is constructed using a basis of  $I$ -splines (and  $M$ -splines) that are supported on the interval  $[0, 1]$ , and with basis coefficients  $\mathcal{W} = \{w_k\}_{k=1}^K$  (which here are not dependent on covariates). The original SPQR method took the basis to have equally-spaced knots on  $[0, 1]$  (Xu and Reich, 2021). To reflect that xSPQR is designed for data with varying degrees of tail-heaviness (which may be covariate dependent), we instead place the knots at a sequence of quantiles with equally-spaced levels in  $[0, 1]$ . The quantiles are estimated empirically using the training response data, and we ensure that knots are always placed at the boundaries of the unit interval.

Figure 1 provides illustrative examples of the distribution and density functions for this flexible SPQR-based bGP model, alongside the constituent SPQR and GP distributions

and density functions. We observe great flexibility in the bulk of the distribution, and the desired exact upper GP tails. As the hyper-parameters  $p_a$  and  $p_b$  have a clear interpretation as the beginning and end of the blending interval, we can dichotomize the density into the “bulk” for  $y < a$ , which is purely driven by SPQR, and the “upper-tail” for  $y \geq b$ , which is driven by both SPQR and  $\xi$ . The hyper-parameters  $c_1$  and  $c_2$  determine the relative weights placed on the constituent distribution functions in (4) during the blending interval. Comparing the first and third rows of Figure 1, we observe that a larger value of  $c_1$ , relative to  $c_2$ , places more weight on the SPQR distribution function when blending. Given that  $F_{\text{SPQR}}(\cdot|\mathcal{W})$  is substantially more flexible than  $F_{\text{GP}}(y|\tilde{u}, \tilde{\sigma}_u, \xi)$ , we consider hereafter only the cases where  $c_1 \geq c_2$ ; for simplicity, we also set  $c_2 = 5$  throughout.

Extending the unconditional model to allow for covariate effects is straightforward. We let  $Y|\mathbf{X} = \mathbf{x} \sim \text{bGP}(\mathcal{W}(\mathbf{x}), \xi(\mathbf{x}))$ , which has conditional distribution function

$$H(y|\mathbf{x}) = \begin{cases} F_{\text{SPQR}}(y|\mathbf{x})^{1-p(y)} F_{\text{GP}}(y|\tilde{u}(\mathbf{x}), \tilde{\sigma}_u(\mathbf{x}), \xi(\mathbf{x}))^{p(y)}, & y > \tilde{u}(\mathbf{x}), \\ F_{\text{SPQR}}(y|\mathbf{x}), & y \leq \tilde{u}(\mathbf{x}), \end{cases} \quad (7)$$

where  $F_{\text{SPQR}}(y|\mathbf{x})$  is as defined in (3). As in (5), the functions  $\tilde{u}(\mathbf{x})$  and  $\tilde{\sigma}_u(\mathbf{x})$  are deterministic functions of  $p_a$ ,  $p_b$ ,  $a = Q_{\text{SPQR}}(p_a|\mathbf{x})$ ,  $b = Q_{\text{SPQR}}(p_b|\mathbf{x})$ , and  $\xi(\mathbf{x})$ ; note that the covariates  $\mathbf{x}$  enter the conditional bGP distribution through both the constituent bulk distribution function,  $F_{\text{SPQR}}(y|\mathbf{x})$ , and the shape parameter of the GP distribution for the upper-tail;  $\xi(\mathbf{x})$  can be represented as a flexible nonlinear function of  $\mathbf{x}$  that is estimated alongside the weights of the conditional bulk distribution. We further note that the weighting function,  $p(y)$ , and its hyper-parameters,  $p_a$ ,  $p_b$ ,  $c_1$ , and  $c_2$ , are not dependent on covariates.

As outlined in (2), the basis weights  $\mathcal{W}(\mathbf{x}) = \{w_k(\mathbf{x})\}_{k=1}^K$  of the conditional density function in the SPQR framework,  $f_{\text{SPQR}}(y|\mathbf{x})$ , are modelled as the final layer of a multi-

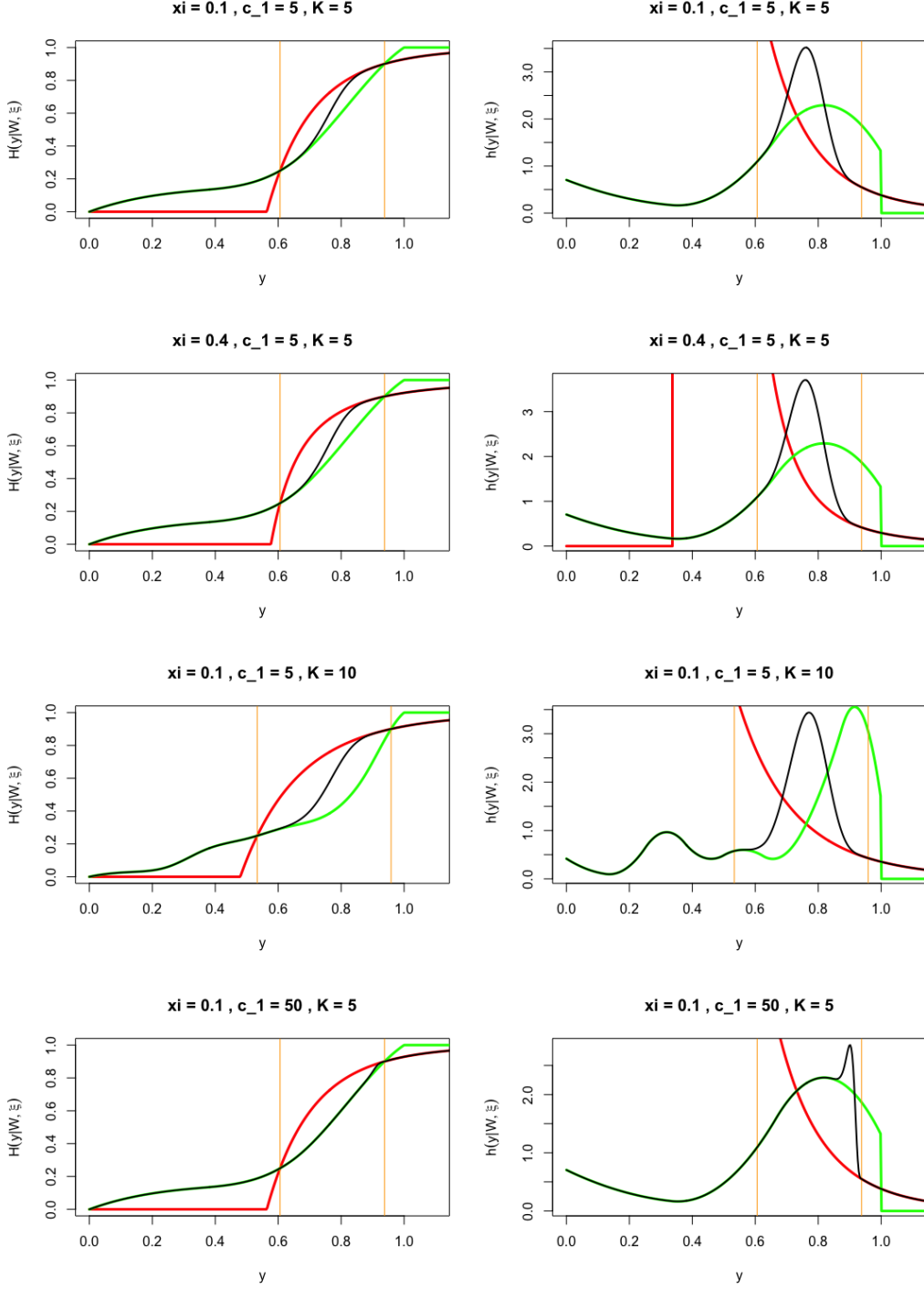


Figure 1: Illustrative examples of the blended GP distribution (left) and density (right) functions, with the constituent distribution modelled via SPQR. For a fixed random seed, we generate  $K$  basis coefficients and construct the SPQR density and distribution functions (green curves). We then find  $a = Q_{\text{SPQR}}(p_a|\mathcal{W})$  and  $b = Q_{\text{SPQR}}(p_b|\mathcal{W})$ , where  $p_a = 0.25$  and  $p_b = 0.9$ . The values of  $a$  and  $b$  are denoted by the orange horizontal lines. Then, we find the required GP distribution function (red) to satisfy continuity of the  $\text{bGP}(\mathcal{W}, \xi)$  distribution function; its resulting distribution and density functions are provided in black. The weighting function shape parameter  $c_2$  is fixed to  $c_2 = 5$  across all panels.

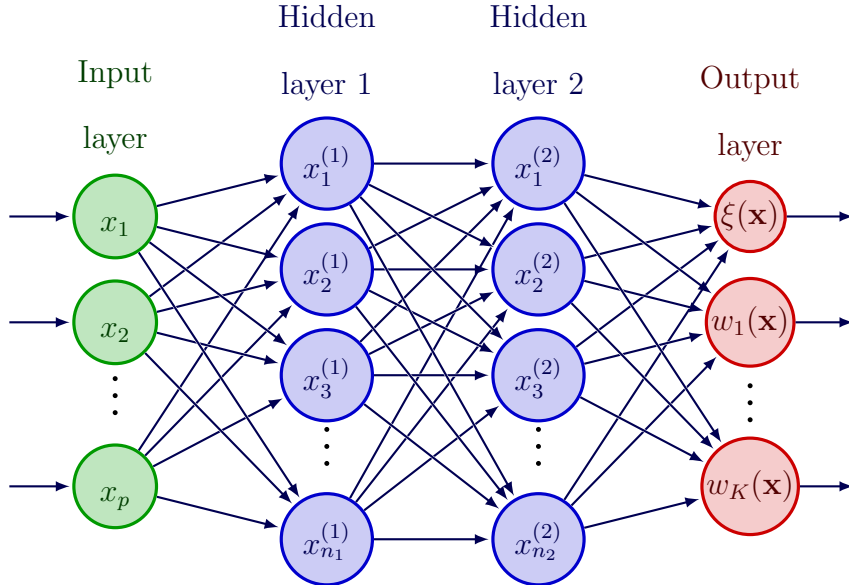


Figure 2: Schematic of the underlying multi-layer perceptron (MLP) of an xSPQR model with  $H = 2$  hidden layers. The input covariates are  $\mathbf{x} = (x_1, \dots, x_p)$ , and the output of the final softmax $^*(\cdot)$  layer is  $(\xi(\mathbf{x}), w_1(\mathbf{x}), \dots, w_K(\mathbf{x}))$ , where  $w_1(\mathbf{x}), \dots, w_K(\mathbf{x})$  are the  $K$  basis functions comprising the constituent SPQR density/distribution.

layer perceptron; a softmax final activation layer is applied to ensure that the  $K$ -vector of weights must sum to one. For xSPQR, we must also model the shape parameter function,  $\xi(\mathbf{x})$ . A natural and parsimonious choice is to combine the modelling of  $\xi(\mathbf{x})$  with that of  $\mathcal{W}(\mathbf{x})$ . To this end, we jointly model  $(\xi(\mathbf{x}), \mathcal{W}(\mathbf{x}))$  as the final layer of a multi-layer perceptron (see Figure 2) with an appropriately chosen final activation layer; we replace the final layer of (2) by

$$(\xi(\mathbf{x}), \mathcal{W}(\mathbf{x})) = \mathbf{x}^{(H+1)} = \text{softmax}^*(\mathbf{W}^{(H+1)}\mathbf{x}^{(H)} + \mathbf{b}^{(H+1)}),$$

where the softmax $^*(\cdot)$  activation function applies a  $\xi$ -specific activation function to the first element of its input vector, and the usual softmax $(\cdot)$  activation to the last  $K$  elements. The  $\xi$ -specific activation function should be chosen to ensure an appropriate range for  $\xi(\mathbf{x})$ , with examples including: exponential ( $\xi(\mathbf{x}) > 0$ ), sigmoid ( $\xi(\mathbf{x}) \in (0, 1)$ ), or tanh ( $\xi(\mathbf{x}) \in (-1, 1)$ ), or scalings thereof; see discussion by Richards and Huser (2024).

Hereon, we refer to this methodology of density regression as extremal SPQR, or

xSPQR. The nomenclature emphasises the flexible distributional assumptions for our density regression model, but we note that alternative models for the body of the data could also be used in combination with the blended GP.

### 3.4 Inference

Inference for xSPQR follows similarly to SPQR, as described in Section 2.2. We use Adam, with default hyper-parameters, to train the MLP that defines the parameter vector  $(\xi(\mathbf{x}), w_1(\mathbf{x}), \dots, w_K(\mathbf{x}))$ , where the loss function is the negative log-likelihood associated with the conditional bGP density in (7). We note that the hyper-parameters of the blending function  $p(y)$  in (4) are fixed during training of the model. Prior to model fitting, observations  $\{(y_i, \mathbf{x}_i)\}_{i=1}^n$  are split into training and test sets,  $\{(y_i, \mathbf{x}_i)\}_{\text{train}}$  and  $\{(y_i, \mathbf{x}_i)\}_{\text{test}}$ , respectively. We assume our observations  $y_i$  satisfy  $y_i > 0, i = 1, \dots, n$ ; however, as the SPQR density is supported on the unit interval, and training response observations  $\{y_i\}_{\text{train}}$  may not fall in  $[0, 1]$ , we must first standardise  $\{y_i\}_{\text{train}}$  to the unit interval via a min-max transformation; this is based on the training data alone. We use the same values to standardise  $\{y_i\}_{\text{test}}$ , however, there are no guarantees that all observations of the resulting standardised test response data will satisfy  $y_i < 1$ . Although this is not an issue for xSPQR, any such test observation cannot be handled by SPQR without re-training of the model, and all associated probability and density estimates will degenerate to one and zero, respectively; examples of this phenomena are illustrated in the application, Section 5.

The xSPQR model is trained using the R interface to **keras** (Allaire and Chollet, 2021). Before training, we further hold out 20% of the training data for validation during optimisation of the MLP. To mitigate overfitting, our training scheme uses checkpoints and early-stopping (Prechelt, 2002). At each iteration of the optimisation algorithm, we evaluate the

negative log-likelihood on the validation data, and then determine the “best fitting” model (over all iterations) as that which minimises the validation loss function. Early-stopping halts the optimisation scheme early if the validation loss has not decreased in the last  $\Delta \in \mathbb{N}$  iterations (we set  $\Delta = 25$  throughout). We also add  $L_1$  penalties to the final activation layer for the shape parameter,  $\xi(\mathbf{x})$ , which provides further model regularisation; see, e.g., Goodfellow et al. (2016).

Courtesy of the modular nature of the xSPQR density, we can use pre-training (see Goodfellow et al. (2016), Ch.8) to increase the computational efficiency of the inference procedure and mitigate numerical instability during training. When fitting the xSPQR model, we first fit the corresponding SPQR model, i.e., with  $p_a = p_b \rightarrow 1$ . We then use the parameters of the estimated neural network as initial estimates when training xSPQR. We find that this procedure works well in practice.

While we presented the xSPQR method in Section 3 for a real-valued shape parameter,  $\xi(\mathbf{x}) \in \mathbb{R}$ , there may be computational and practical benefits to constraining  $\xi(\mathbf{x})$  to be non-negative. When the shape parameter  $\xi(\mathbf{x})$  is negative, the resulting GP distribution has a finite upper endpoint, which can make validation and testing of GP regression models computationally troublesome. If test or validation response data are observed to exceed their predicted upper-endpoint, then the negative log-likelihood function will evaluate to a non-finite value and, as a consequence, the loss surface is highly non-regular; iterative stochastic gradient descent methods (e.g., Adam) may then struggle to find global maxima. For a discussion of this issue, particularly with respect to deep GP regression models, see Richards and Huser (2022, 2024). For simplicity, we hereafter constrain  $\xi(\mathbf{x}) \in (0, 1)$  using the sigmoid activation function in the final layer of the MLP; the choice to constrain  $\xi(\mathbf{x}) < 1$  is judicious, and is motivated primarily by the typical values of  $\xi(\mathbf{x})$  found in

applications of GP regression models.

### 3.5 Relative variable importance for xSPQR

As with many applications of density regression models, we seek to assess the relative importance of covariates on determining the conditional distribution. In the xSPQR framework, the parameters of the conditional density comprise those that influence the bulk (i.e.,  $\mathcal{W}(\mathbf{x})$ ) and those that are specific to the tails (i.e.,  $\xi(\mathbf{x})$ ). Thus, xSPQR permits the covariates to separately affect the body and the tail of the conditional distribution; as a result of this, we may expect the relative importance of covariates to change between the bulk and tails.

Following the discussion in Section 2.3, we assess relative importance in the bulk by estimating the VI scores for a sequence of  $\tau$  values; recall that, for  $\tau < p_a$ , the conditional distribution function for the xSPQR model is exactly that of the usual SPQR framework. When considering relative importance in the tails, we have two options: i) considering VI scores for  $\tau$  close to one or ii) directly interpreting relative importance for the shape parameter,  $\xi(\mathbf{x})$ ; the latter can be achieved similarly to the conditional quantile function (for fixed  $\tau$ ), by setting  $g(\mathbf{x})$  in (2.3) to be  $\xi(\mathbf{x})$ .

## 4 Simulation Study

### 4.1 Overview

Here we provide a simulation study to showcase the benefits of using xSPQR over SPQR when extrapolating into the tails. Covariates  $\mathbf{X}_i, i = 1, \dots, 3$ , are drawn independently from a  $\text{Unif}(0,1)$  distribution. We then draw our response  $Y \mid (\mathbf{X} = \mathbf{x})$  from a log-normal distribution with density function  $f(y|\mathbf{x}) = (\sqrt{2\pi}\sigma(\mathbf{x})y)^{-1} \exp\{-(\log y - \mu(\mathbf{x}))^2/(2\sigma^2(\mathbf{x}))\}$

for  $y > 0$ ,  $\sigma(\mathbf{x}) > 0$ , and  $\mu(\mathbf{x}) \in \mathbb{R}$ . The parameters  $\mu(\mathbf{x})$  and  $\sigma(\mathbf{x})$  are dependent on  $\mathbf{x}$ , and we set  $\mu(\mathbf{x}) = 5(1 - 1/(1 + \exp(-(1 - 5x_1 x_2))))$  and  $\sigma(\mathbf{x}) = 1/(1 + \exp(-(1 - 5x_1 x_2)))$ ; hence only  $X_1$  and  $X_2$  act on  $Y$ .

To evaluate the efficacy of conditional density estimation, we compute the integrated conditional 1-Wasserstein distance (IWD), defined by

$$\text{IWD} = \int_{\mathcal{X}} \int_0^1 |Q(y|\mathbf{x}) - \hat{Q}(y|\mathbf{x})| d\mathbf{x},$$

where  $Q(y|\mathbf{x})$  denotes the true conditional quantile function (and  $\hat{Q}(y|\mathbf{x})$  denotes its estimate), and where  $\mathcal{X}$  denotes the sample space for the covariate vector  $\mathbf{X}$  (in the above case,  $\mathcal{X} = [0, 1]^3$ ). We estimate the IWD out-of-sample by generating a test set of 5000 covariate vectors and performing Monte-Carlo integration. We also consider a tail-calibrated version of the IWD, denoted by tIWD, which is constructed by replacing the limits of the inner integral of (4.1) with  $[0.999, 1]$ .

We perform 100 experiments; for each, we generate  $n \in \{1000, 10000\}$  samples from the aforementioned log-normal regression model, and fit the original SPQR and our xSPQR models. We consider a coarse grid of hyper-parameters for the two models, which was motivated by unreported initial experiments. For the  $M$ -spline basis and underlying MLP (of both models), we consider  $K \in \{15, 25\}$  basis functions, a 2-layered neural network with  $n_h \in \{16, 32\}$  nodes per layer, and two activation functions  $\phi(\cdot)$ : sigmoid and ReLU. For the hyper-parameters specific to xSPQR, we consider  $p_a \in \{0.75, 0.9, 0.925\}$ ,  $p_b \in \{0.95, 0.99, 0.999\}$ , and  $c_1 \in \{5, 25\}$ . The  $\xi$ -specific activation function is taken to be a sigmoid activation, scaled such that  $\xi(\mathbf{x}) \in (0, 0.5)$ .

Table 1: Results of the simulation study. The median of the IWD and tIWD estimates (alongside 50% confidence intervals; in brackets) are reported for the original SPQR and new xSPQR models, with values for the latter in bold. The hyper-parameters of the xSPQR,  $(p_a, p_b, c_1)$ , are optimised for each row by minimising the tIWD, and are reported in the final column.

	$n$	$K$	$n_h$	IWD	tIWD	Optimal $(p_a, p_b, c_1)$
1000	15	16	5.61 (5.48, 5.76)/ <b>3.47</b> (3.30, 3.62)	11.2 (10.3, 12.3) / <b>9.23</b> (7.99, 10.6)	(0.9, 0.999, 5)	
	15	32	4.62 (4.53, 4.70)/ <b>3.06</b> (2.96, 3.26)	9.50 (8.63, 10.6) / <b>9.66</b> (8.18, 11.2)	(0.925, 0.999, 5)	
	25	16	5.75 (5.63, 5.94)/ <b>2.96</b> (2.83, 3.12)	12.0 (11.2, 13.0)/ <b>9.56</b> (8.42, 10.9)	(0.925, 0.999, 5)	
	25	32	4.38 (4.32, 4.48)/ <b>2.35</b> (2.22, 2.54)	9.20 (8.31, 9.96)/ <b>9.80</b> (8.70, 11.1)	(0.925, 0.999, 5)	
	15	16	1.86 (1.79, 1.90)/ <b>1.67</b> (1.63, 1.73)	10.6 (9.51, 11.3)/ <b>7.08</b> (6.40, 7.85)	(0.75, 0.99, 25)	
	15	32	1.83 (1.79, 1.91)/ <b>1.68</b> (1.61, 1.75)	10.7 (10.0, 11.6)/ <b>6.99</b> 6.36, 8.05)	(0.75, 0.99, 25)	
10000	25	16	1.00 (0.95, 1.07)/ <b>0.80</b> (0.76, 0.84)	8.60 (7.33, 10.0)/ <b>5.56</b> (4.45, 6.86)	(0.75, 0.99, 25)	
	25	32	1.01 (0.95, 1.08)/ <b>0.79</b> (0.76, 0.84)	10.2 (9.40, 16.6)/ <b>5.29</b> (4.59, 6.50)	(0.75, 0.99, 25)	

## 4.2 Results

Table 1 provides the results of the simulation study. For brevity, we present here only the results when  $\phi(\cdot)$  in (2) is the sigmoid activation; this provided consistently better results compared to the ReLU activation function. We observe that xSPQR consistently provides lower IWD and tIWD estimate than the competing SPQR method, which illustrates the efficacy of xSPQR for modelling heavy-tailed conditional densities. As one might expect, the estimation accuracy tends to increase with the number of knots and the number of nodes in the underlying MLP. For the optimal hyper-parameters, we find a lower  $c_1$  is preferred in a low sample setting, whilst a higher  $c_1$  is preferred when more data are available for inference. As discussed alongside Figure 1, a higher value of  $c_1$  puts more weight on the more flexible SPQR distribution during blending; this may be preferable when you have more data available to infer this component of the model. For the blending interval, we find consistent agreement, when  $n = 10000$ , that the preferred blending quantile levels are  $p_a = 0.75$  and  $p_b = 0.99$ ; this provides a relatively wide interval for blending of the two constituent distribution functions, with the exact GP upper-tails beginning at  $b$ . Although Table 1 provides some intuition as to appropriate choices of hyper-parameters for xSPQR, it is by no means conclusive. We advocate that, in practice, a grid-search over hyper-parameters is performed and the quality of xSPQR fits are compared on hold-out data.

Figure 3 compares out-of-sample density and distribution estimation using SPQR and xSPQR. In this case, we take model fits to  $n = 10000$  samples, using the optimal hyper-parameters from the bottom row of Table 1. As Figure 3 illustrates, xSPQR is much better able to capture the upper-tails of the true log-normal distribution function. Moreover, SPQR is unable to provide any useful estimates of the conditional distribution function for

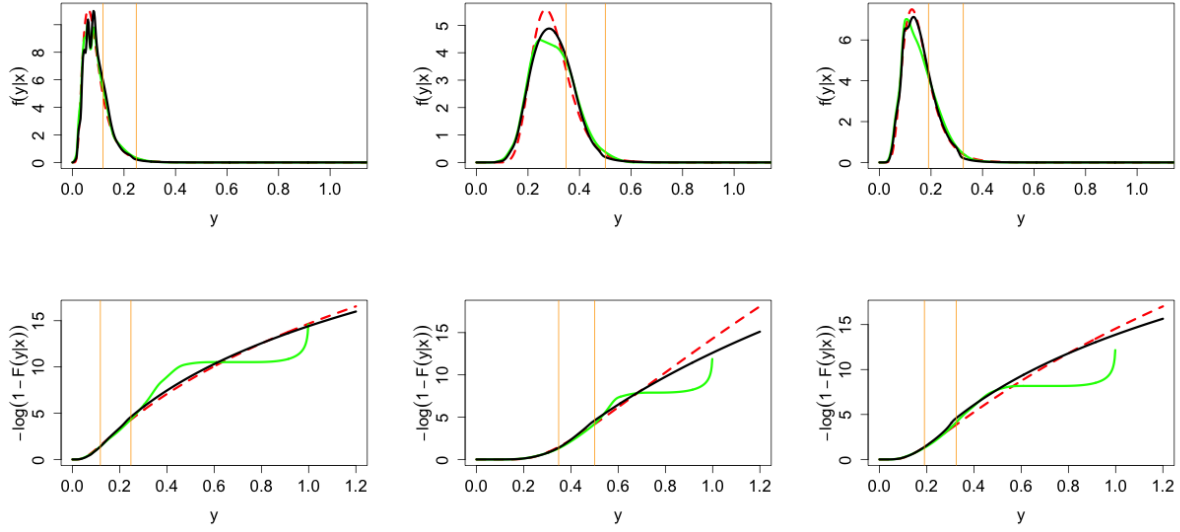


Figure 3: Simulation study: estimates of density (top) and log-survival (bottom) functions for three test covariate vectors. The red dashed lines give the true functions; the black and green curves are the corresponding estimates from SPQR and xSPQR, respectively. The values of  $a$  and  $b$  (from the xSPQR fit) are denoted by the orange horizontal lines.

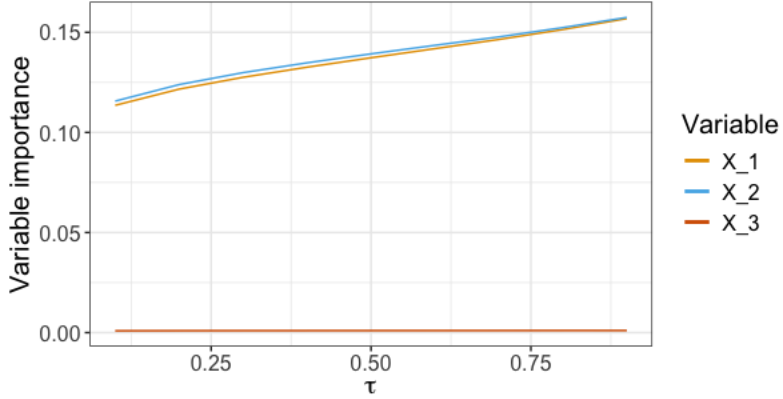


Figure 4: Simulation study: estimates of the variable importance scores  $VI_j(\hat{Q}(\tau|\mathbf{x}))$  for the covariates  $X_j, j = 1, 2, 3$ , as a function of the quantile level  $\tau$ .

$y > 1$ . Figure 4 also provides estimates of the variable importance scores from the aforementioned fitted xSPQR model. Specifically, we estimate  $VI_j(\hat{Q}(\tau|\mathbf{x}))$  where the function of interest  $g(\cdot)$ , defined in 5, is taken to be the estimated conditional  $\tau$ -quantile function. The estimates are able to capture the true underlying covariate importance, specifically that  $X_3$  does not have any effect on the conditional distribution at any quantile level  $\tau$ , whilst  $X_1$  and  $X_2$  have an equal effect for all values of  $\tau$ . The  $\xi$ -specific variable importance

scores (see Section 3.5) are in agreement; their estimates are 0.0156, 0.0234, 0.0009 for  $X_1$ ,  $X_2$ , and  $X_3$ , respectively.

## 5 Application to U.S. wildfire burnt areas

We demonstrate the flexibility of xSPQR by modelling U.S. wildfire burnt areas, that were originally compiled and analysed by Lawler and Shaby (2024). The data consist of burnt areas (in 1000s of acres) and counts for over 10,000 wildfires across the contiguous U.S., from 1990 to 2020; only fires exceeding 1000 acres of burnt area are included in the dataset. The dataset includes several covariates, including spatio-temporal coordinates, meteorological variables, fire weather indices, and housing density. Lawler and Shaby (2024) studied these data using a joint model for counts and area with spatial random effects, and employed the extended GP distribution for modelling burnt areas. In our work, we focus on modelling the distribution of the continuous burnt areas, conditional on the following 6 covariates: year (`fire_yr`), total precipitation during the month of the fire (`pr_curr`; mm) and during the entire previous year (`pr_prev`; mm), minimum relative humidity (`rmin`; %-age), maximum temperature (`tmax`; K), and windspeed (`wspd`; m/s). The final three variables (`rmin`, `tmax`, `wspd`) are aggregated into their monthly means.

Following Lawler and Shaby (2024), we split the data into training and testing sets of 6416 and 3344 fires, respectively. The split is not random, as the test set consists of the first and last five years of the data: 1184 fires from 1990 to 1994, inclusive, and 2160 fires from 2016 to 2020, inclusive. Additionally, we uniformly-at-random select 20% of the training data for validation during training of the xSPQR model; see Section 3.4. As illustrated by Richards and Huser (2022) and Lawler and Shaby (2024), U.S. wildfire burnt areas are extremely heavy-tailed ( $\xi > 0.5$ ), which can cause numerical difficulties during

training of deep extreme quantile regression models (Richards and Huser, 2022). While Lawler and Shaby (2024) employ a log-transform of the data to mitigate this issue, we instead follow Richards and Huser (2022) and model the square-root of the burnt areas as our response variable,  $Y$ ; the square-root transformation better preserves the tail behavior of the response compared to the log-transform, and can be interpreted as the diameter of an affected region. The wildfires are assumed to be independent of each other; while a naive assumption, it is nevertheless aligned with our specific goal of testing the appropriateness of the xSPQR framework for density regression.

We fit and compare both the original SPQR and the EVT-compliant xSPQR models to the data. When deciding on the optimal hyper-parameters for the SPQR/xSPQR model, we perform a coarse grid search over hyper-parameters to choose their optimal values; we use the same MLP architecture for both frameworks. The candidate models are compared using the negative log-likelihood (evaluated on the test data) and by visual examination of a model diagnostic, the pooled QQ plot which is to be discussed. The optimal neural network comprising our SPQR/xSPQR model has  $H = 2$  hidden layers, each with  $n_h = 12$  nodes, and with  $K = 25$  basis functions describing the body of the distribution. An exploratory data analysis, whereby we fit stationary GP models to the response data, reveals that the response burnt area data are in fact heavy-tailed, with the vast majority of fits returning estimates of  $\xi$  exceeding zero. As such, we constrain  $\xi(\mathbf{x}) > 0$  for xSPQR by using the logistic activation function. For the blending interval, we set  $p_a$  and  $p_b$  to be 0.9 and 0.999, respectively. Finally,  $c_1$  and  $c_2$  are set to be 25 and 5, respectively, with these two values being carried over from our numerical studies.

The covariates for both the training and test sets are normalised by subtracting and dividing by the marginal mean and standard deviation vectors, respectively, of the training

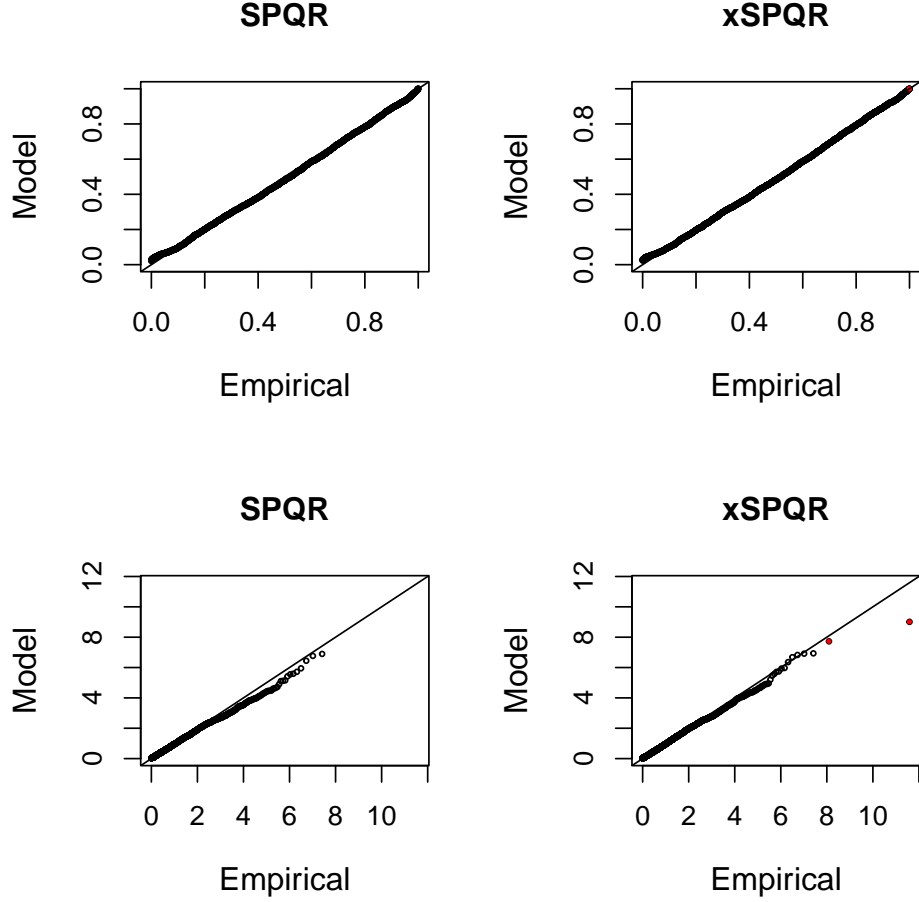


Figure 5: Goodness-of-fit diagnostics for the SPQR and xSPQR models. Pooled PP (top) and QQ (bottom) plots for the fitted SPQR (left) and xSPQR (right) models, evaluated on the test data. The red points in the right column denote the two most extreme test values, which cannot be modelled using SPQR and thus do not appear on the left column.

covariate data. Similarly, the response data are scaled to  $[0, 1]$  using the min-max transformation, as described in Section 3.4. As a consequence, there are two response values in the scaled test data which exceed one, corresponding to the two largest wildfires across the entire dataset, which occurred in 2017 and 2020. As explained in Section 3.4, regular SPQR can not provide any usable estimates for these particularly extreme test values, but this is not an issue for xSPQR.

Figure 5 provides visual goodness-of-fit diagnostics for the fitted SPQR and xSPQR models. We create out-of-sample pooled PP and QQ plots, whereby the fitted conditional

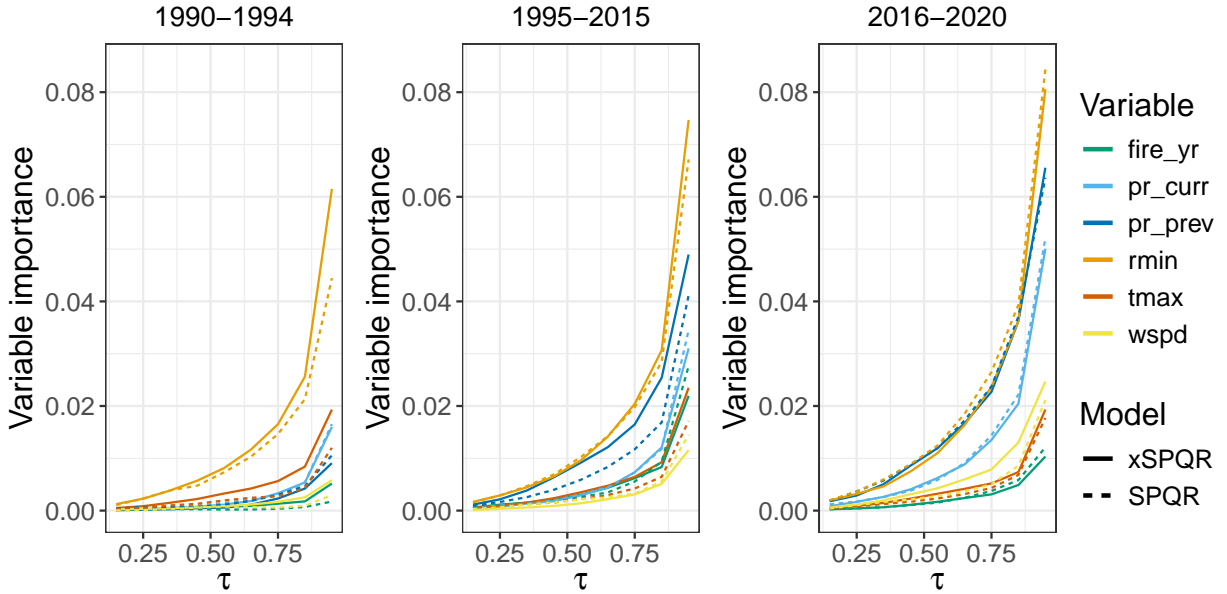


Figure 6: Estimates of the variable importance scores  $VI_j(\hat{Q}(\tau|\mathbf{x}))$  as a function of the quantile level  $\tau$ . Different colours correspond to different covariates, while the dashed and solid lines correspond to estimates from SPQR and xSPQR, respectively. The left and right panels correspond to the two test periods: 1990–1994 and 2016–2020, respectively; the central panel corresponds to the training period, 1995–2015.

models are used to transform the test data onto standard (unconditional) margins. The top row of PP plots are on uniform margins which showcase goodness-of-fit for the entire distribution, while the bottom row QQ plots are on exponential margins, to highlight the fits in the upper-tails (see, e.g., Heffernan and Tawn, 2001); deviation of points from the diagonal suggest poor fits. Both SPQR and xSPQR provide fantastic fits for the entire range of the data, however, xSPQR gives markedly better fits in the upper-tails, as the model is better designed to handle extreme events. Moreover, xSPQR is capable of predicting well the probability of the two most extreme burnt areas in the test data; SPQR is unable to provide any usable estimates for these events.

Figure 6 provides estimates of the variable importance scores for both the SPQR and xSPQR model fits. We consider three time periods: the two test periods, 1990–1994 and 2016–200, and the training period, 1995-2015. Across both models and all time periods,

minimum relative humidity  $r_{\min}$  is identified as the most important variable for predicting the distribution of U.S. wildfire burnt areas across all quantile levels,  $\tau$ . Additionally, while precipitation appears less important than maximum temperature ( $t_{\max}$ ) in the period 1990–1994, both current ( $pr\_curr$ ) and previous year ( $pr\_prev$ ) precipitation show significant increases in relative importance of these variables between 1995 and 2020, with both overtaking maximum temperature during this period. The covariates windspeed ( $wspd$ ) and year ( $fire\_yr$ ) remain relatively unimportant throughout the entire time period. This suggests that dryness is a bigger driving factor of burnt area than high temperatures: this is not surprising, as while high temperatures increase ignition rates (from natural causes) and windspeed affects the rate of spread, dryness is directly tied to the total area that has potential for burning. Figure 6 also illustrates an overall increase in the VI scores over time, suggesting that these meteorological variables may be becoming increasingly more important. Table 2 provides the variable importance scores for the shape parameter  $\xi$ , for each of the three time periods. The most important variable for estimating  $\xi$  is the previous years' precipitation,  $pr\_prev$ . Our interpretation is that while low humidity leads to more burnt area (as  $r_{\min}$  is in the top three most important variables for the tail), the most devastating wildfires, in terms of burnt area, depend more on whether the region has been dry for prolonged periods of time. On the other hand, the year is estimated to be largely inconsequential for determining the tail of the conditional density. Beyond this, the results are largely consistent with the relative variable importance analysis for the body of the distribution. Overall, across the body and the tails, we identify dryness as having the largest effect on the distribution of U.S. wildfire burnt areas.

Figure 7 provides the density of  $\xi(\mathbf{x})$  estimates for the training period, 1995–2015, and the two testing periods of 1990–1994 and 2016–2020. Figure 7 illustrates a positive temporal

Table 2: Estimates of the variable importance scores for the shape parameter,  $\xi(\mathbf{x})$ , of the xSPQR model fit.

Time period	pr_prev	rmin	tmax	wspd	pr_curr	fire_yr
<b>1990–1994</b>	2.35	2.08	1.41	0.90	0.91	0.22
<b>1995–2015</b>	2.87	2.13	1.82	1.72	1.21	0.61
<b>2016–2020</b>	2.39	1.69	1.42	2.26	1.58	0.50

trend in the estimates. The change is most noticeable between 1990–1994 and 1995–2015, and may suggest that U.S. wildfires are becoming more heavy-tailed, i.e., extreme, over time. While the estimates for 2016–2020 are more concentrated compared to the training period, they are both centered around approximately the same value. We note that the response data have undergone a square-root transformation, and a value of  $\xi(\mathbf{x}) > 0.25$  on the response scale would translate to approximately  $\xi(\mathbf{x}) > 0.5$  on the original scale; in the latter case, the blended GP density does not have finite variance, which suggests that the original response data are extremely heavy-tailed.

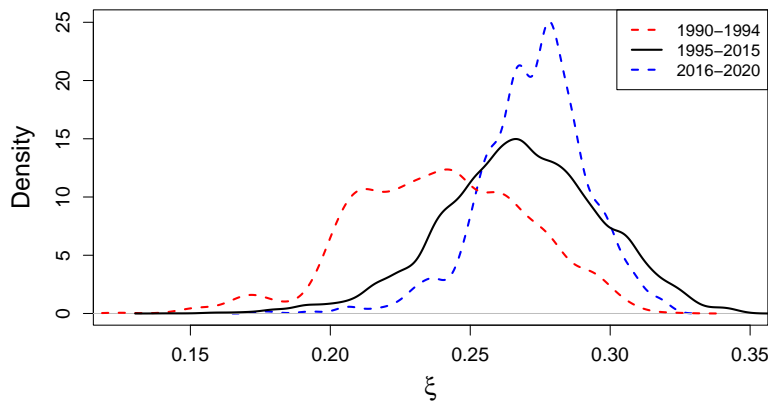


Figure 7: Density of the estimated shape parameter values,  $\xi(\mathbf{x})$ , stratified by time period.

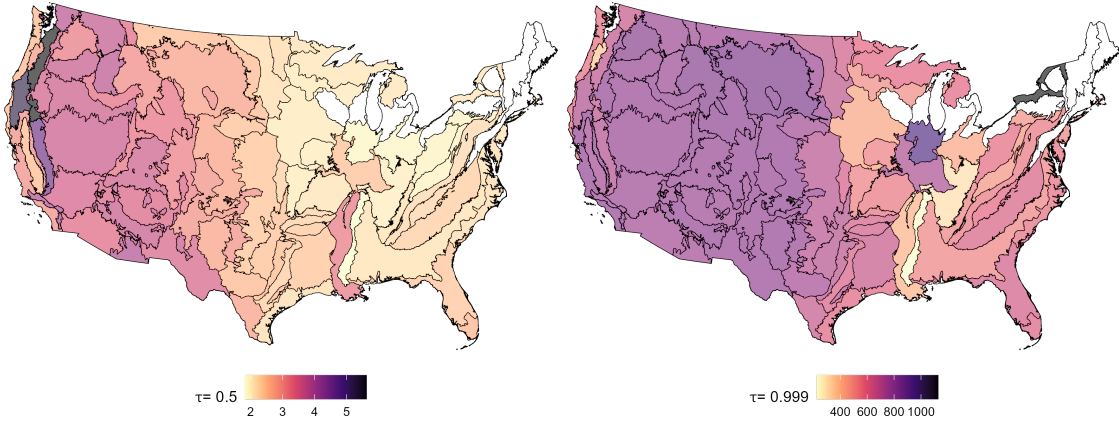


Figure 8: Estimates of the median (left) and 0.999-quantile (right) of burnt area (in 1000s of acres) for all observed wildfires, averaged over each L3 ecoregion. Transparent regions do not include any observed wildfires.

Figure 8 illustrates the spatial variability in the estimated quantiles of the burnt area response. For each fire in the dataset, we estimate the median and 0.999-quantile using the fitted xSPQR model; the former quantity is estimated via the SPQR model for the bulk while the latter is estimated via the GP model for the upper tail. The quantile is squared to obtain the actual burnt area in 1000s of acres, and then aggregated over Level III (L3) ecoregions. The ecoregions group ecosystems that are similar in terms of their biotic, abiotic, terrestrial, and aquatic ecosystem components, including human activity (McMahon et al., 2001; Omernik and Griffith, 2014); ecoregion boundaries are made available by the U.S. Environmental Protection Agency<sup>1</sup>, with lower levels indicating more aggregation (and therefore larger ecoregions). From Figure 8, estimates of the quantiles show spatial variability across the country, with higher values concentrated in the western regions of the U.S. The illustrated east-west gradient is more pronounced in the map of the estimated 0.999-quantile than the median; alongside the differences in the relative VI scores for the bulk and tail (see Figure 6 and Table 2), the differences in the spatial patterns of the median and tail quantiles provides further evidence that the covariates have different

<sup>1</sup><https://www.epa.gov/eco-research/level-iii-and-iv-ecoregions-continental-united-states>

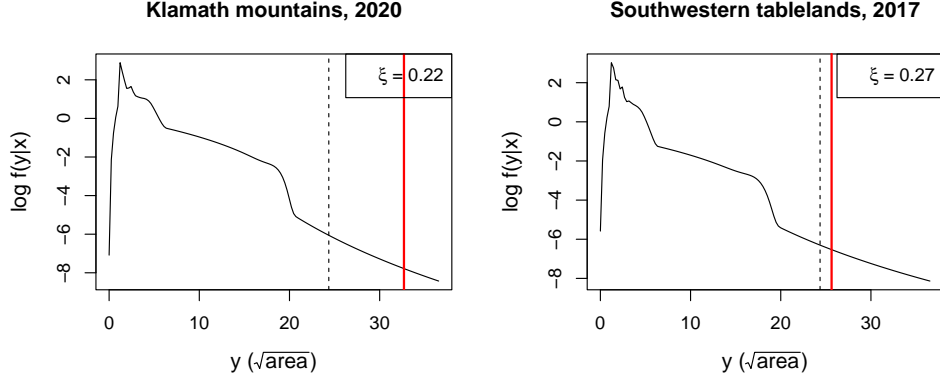


Figure 9: Estimated conditional log-density functions  $\log f(y|x)$  for the two largest wildfires in the dataset. The response variable  $Y$  is the square-root burnt area, which were originally measured in 1000s of acres. The red lines denote the observed value for the fires, while the dashed black lines represent the largest value that is observed in the training data.

impacts on the bulk and upper-tail of the wildfire distribution.

Finally, we focus on the two most extreme fires in the dataset (in terms of burnt area). We refer to them as the Klamath mountains and Southwestern tablelands fires, based on their L3 ecoregion of occurrence (Lawler and Shaby, 2024). As mentioned above, they are both present in the second test period, 2016–2020, and are therefore outside the range of the training data used to fit our models. Both fires were associated with moderate temperatures ( $< 30^\circ\text{C}$ ), but with very low humidity ( $< 25\%$ ). Additionally, in the case of the Klamath mountains fire, the aggregate precipitation over the past month (`pr_curr`) was in the lowest 0.07 quantile of the training data. Figure 9 provides the xSPQR estimates of the conditional log-density for these two fires. In each case, the observed wildfires are well beyond the observed maximum of the training data, and are modelled explicitly by the GP upper-tail of the xSPQR model. The estimated shape parameters for these two fires, while high, are lower than the median and 0.8 quantile, respectively, of the entire test set of  $\xi$  predictions. Figure 9 highlights the flexibility of the xSPQR model; unlike existing fully-parametric bulk and tail models (see Section 1), xSPQR is able to capture both the

heavy-tails and high kurtosis exhibited by the data.

## 6 Discussion

In this work, we developed a flexible framework for conditional bulk and tail estimation called extremal semi-parametric quantile regression (xSPQR). To achieve this, we propose the blended generalised Pareto (bGP) distribution, which is a new univariate model for the entire range of data that is EVT-compliant, in that its upper-tail follows exactly a GP distribution. We use the bGP distribution to combine a deep parametric GP regression model with the traditional SPQR framework for conditional density estimation. The flexible nature of SPQR ensures that parametric assumptions do not need to be made about the bulk of the conditional distribution, which can instead be arbitrarily flexible. The xSPQR framework addresses one of the main weaknesses of SPQR by allowing the modelling of heavy-tailed distributions and making predictions outside the range of the observed data. We also obtain variable importance estimates for xSPQR using accumulated local effects; as xSPQR allows covariates to separately affect the bulk and the tail of the distribution, we can perform inference on variable importance for the tails separately of that for the bulk. A simulation study and a real-data application to U.S. wildfire burnt areas demonstrated the efficacy of xSPQR.

In our current work, the hyper-parameters of the blending function,  $(p_a, p_b, c_1, c_2)$ , are carefully chosen using numerical experiments and via grid search algorithms. Arbitrarily choosing these hyper-parameters can lead to pathological cases where the density function,  $h(y|\mathcal{W}, \xi)$  in (6), is negative for  $y$  in the blending interval,  $[a, b]$ . In practice, we found that this phenomenon was extremely rare, and the risk of it occurring during training of the xSPQR model was mitigated by the use of model pre-training (Section 3.4); however,

future work will investigate regularization techniques for fully precluding this phenomenon.

In this work, we only considered estimation of heavy upper-tails, i.e.,  $\xi(\mathbf{x}) > 0$ ; this constraint was imposed to prevent numerical problems when fitting the xSPQR model. While theoretically xSPQR can handle  $\xi(\mathbf{x}) < 0$ , and we thus presented the blended GP in Section 3.2 for general  $\xi \in \mathbb{R}$ , training of xSPQR in this case requires a much more involved numerical optimisation scheme or reparameterisation of the model; see, e.g., Pasche and Engelke (2024) and Mackay et al. (2024). We leave such a consideration as future work.

Another simple extension of the xSPQR framework is to allow for different subsets of variables to affect the bulk and upper-tail of the distribution, which can be achieved by modelling  $\mathcal{W}(\mathbf{x})$  and  $\xi(\mathbf{x})$  in (7) using separate neural networks (with separate inputs). Further work may also consider a blended GP distribution and resulting xSPQR model that allows for extrapolation in both the lower- and upper-tail of the conditional distribution. An extension of (4), which blends a constituent model for the bulk with two independent GP distributions for the lower- and upper-tail, is trivial; however, inference for such a model using deep learning may be numerically difficult.

## Declarations

### Ethical Approval

Not Applicable

### Availability of supporting data

### Competing interests

The authors have no relevant financial or non-financial interests to disclose.

## Funding details

The authors have no relevant funding details to disclose.

## Acknowledgments

The authors thank Elizabeth S. Lawler for access to the wildfire burnt areas data and for help creating the maps. The authors also thank Brian J. Reich and members of the Glasgow-Edinburgh Extremes Network (GLE<sup>2</sup>N; [glen-scotland.github.io/glen/](https://glen-scotland.github.io/glen/)) for helpful feedback. This work has made use of the resources provided by the Edinburgh Compute and Data Facility (ECDF) ([www.ecdf.ed.ac.uk/](https://www.ecdf.ed.ac.uk/)).

## Appendix

### A Construction of $M$ - and $I$ -splines

A polynomial spline is a piecewise polynomial function over a compact interval, say  $[L, U]$ , with the constituent polynomials having the same degree and connecting smoothly at predetermined knots. Several classes of splines, e.g.,  $B$ -splines, also constitute basis functions of their function space (Prautzsch et al., 2002). Similarly, the  $M$ -spline family of basis functions,  $\{M_k\}_{k=1}^K$ , is suited to representing densities (Curry and Schoenberg, 1966). The  $M$ -splines are piecewise polynomial functions of order  $d$ , which are defined on a set of  $K+d$  knots,  $t_1, \dots, t_{K+d}$ ; the basis function  $M_k(y)$  is positive on  $(t_k, t_{k+d})$ , and zero otherwise. Additionally  $\int_L^U M_k(y)dy = 1$ , which gives  $M_k(y)$  a natural interpretation as a density function supported on  $[L, U]$ . The basis functions are computed using the following system

of recursive equations: for  $d = 1$ ,

$$M_k(y|d) = \begin{cases} \frac{1}{t_{k+1}-t_k}, & t_k \leq y < t_{k+1}, \\ 0, & \text{otherwise.} \end{cases}$$

and, for  $d > 1$ ,

$$M_k(y|d) = \frac{d[(y - t_k)M_k(y|d-1) + (t_{k+d} - y)M_{k+1}(y|d-1)]}{(d-1)(t_{k+d} - t_k)}.$$

In the case of SPQR, we use an order of  $d = 3$  for the polynomial basis. We note that  $B$ -splines are also closely related to  $M$ -splines, as the  $B$ -spline basis function is defined by  $B_k = (t_{k+d} - t_k)M_k/d$  (Ramsay, 1988).

Ramsay (1988) also introduced integrated splines, or  $I$ -splines, over  $[L, U]$ . These are built using basis functions

$$I_k(y|d) = \int_L^y M_k(u|d)du.$$

As each  $M_k(y)$  is a polynomial spline (for  $d > 1$ ) that has the properties of a density function, the corresponding  $I$ -spline has a natural representation as the corresponding distribution function;  $I$ -splines are integrals over  $M$ -splines, and are monotone due to their construction.

Since the  $M$ -splines form a basis, for a vector of weights,  $\mathcal{W} = (w_1, \dots, w_K)$ , the convex combination  $\sum_{k=1}^K w_k M_k(y)$  is also an  $M$ -spline and a valid density function. Therefore, with an appropriate choice of  $\mathcal{W}$ , the  $M$ -splines can be used to model univariate density functions in a semi-parametric manner. In the case where covariate information is available, one can allow  $\mathcal{W}$  to depend on covariates, and construct a representation for conditional density functions; see Section 2 of the main text.

# References

Abrahamowicz, M., Clampl, A., and Ramsay, J. O. (1992). Nonparametric density estimation for censored survival data: Regression-spline approach. *Canadian Journal of Statistics*, 20(2):171–185.

Allaire, J. and Chollet, F. (2021). *keras: R Interface to ‘Keras’*. R package version 2.7.0.

Apley, D. W. and Zhu, J. (2020). Visualizing the effects of predictor variables in black box supervised learning models. *Journal of the Royal Statistical Society: Series B (Methodology)*, 82:1059–1086.

Behrens, C. N., Lopes, H. F., and Gamerman, D. (2004). Bayesian analysis of extreme events with threshold estimation. *Statistical modelling*, 4(3):227–244.

Carreau, J. and Bengio, Y. (2007). A hybrid Pareto model for conditional density estimation of asymmetric fat-tail data. In *Artificial Intelligence and Statistics*, pages 51–58. PMLR.

Castro-Camilo, D., Huser, R., and Rue, H. (2019). A spliced gamma-generalized Pareto model for short-term extreme wind speed probabilistic forecasting. *Journal of Agricultural, Biological and Environmental Statistics*, 24(3):517–534.

Castro-Camilo, D., Huser, R., and Rue, H. (2022). Practical strategies for generalized extreme value-based regression models for extremes. *Environmetrics*, 33(6):e2742.

Chavez-Demoulin, V. and Davison, A. C. (2005). Generalized additive modelling of sample extremes. *Journal of the Royal Statistical Society Series C: Applied Statistics*, 54(1):207–222.

Chavez-Demoulin, V. and Guillou, A. (2018). Extreme quantile estimation for  $\beta$ -mixing time series and applications. *Insurance: Mathematics and Economics*, 83:59–74.

Chui, C., Smith, P., and Ward, J. (1980). Degree of  $L_p$  approximation by monotone splines. *SIAM Journal on Mathematical Analysis*, 11(3):436–447.

Cisneros, D., Richards, J., Dahal, A., Lombardo, L., and Huser, R. (2024). Deep graphical regression for jointly moderate and extreme Australian wildfires. *Spatial Statistics*, 59:100811.

Coles, S. (2001). *An introduction to statistical modeling of extreme values*, volume 208. Springer.

Curry, H. B. and Schoenberg, I. J. (1966). On polya frequency functions IV: The fundamental spline

functions and their limits. *Journal d'Analyse Mathematique*, 17(1):71–107.

Daouia, A., Gardes, L., Girard, S., and Lekina, A. (2011). Kernel estimators of extreme level curves. *Test*, 20(2):311–333.

Daouia, A., Girard, S., and Stupler, G. (2019). Extreme m-quantiles as risk measures: From L1 to Lp optimization. *Bernoulli*, 25(1):264–309.

Daouia, A., Padoan, S. A., and Stupler, G. (2024). Optimal weighted pooling for inference about the tail index and extreme quantiles. *Bernoulli*, 30(2):1287–1312.

Daouia, A., Stupler, G., and Usseglio-Carleve, A. (2023). Inference for extremal regression with dependent heavy-tailed data. *The Annals of Statistics*, 51(5):2040–2066.

Davison, A. C. and Smith, R. L. (1990). Models for exceedances over high thresholds. *Journal of the Royal Statistical Society Series B: Statistical Methodology*, 52(3):393–425.

de Melo Mendes, B. V. and Lopes, H. F. (2004). Data driven estimates for mixtures. *Computational statistics & data analysis*, 47(3):583–598.

Farkas, S., Heranval, A., Lopez, O., and Thomas, M. (2024). Generalized Pareto regression trees for extreme event analysis. *Extremes*, 27(3):437–477.

Farkas, S., Lopez, O., and Thomas, M. (2021). Cyber claim analysis using generalized Pareto regression trees with applications to insurance. *Insurance: Mathematics and Economics*, 98:92–105.

Frigessi, A., Haug, O., and Rue, H. (2002). A dynamic mixture model for unsupervised tail estimation without threshold selection. *Extremes*, 5:219–235.

Gardes, L. and Stupler, G. (2019). An integrated functional weissman estimator for conditional extreme quantiles. *REVSTAT-Statistical Journal*, 17(1):109–144.

Gnecco, N., Terefe, E. M., and Engelke, S. (2024). Extremal random forests. *Journal of the American Statistical Association*, 119(548):3059–3072.

Goodfellow, I., Bengio, Y., and Courville, A. (2016). *Deep learning*. MIT press.

Greenwell, B. M., Boehmke, B. C., and McCarthy, A. J. (2018). A simple and effective model-based variable importance measure. *arXiv preprint arXiv:1805.04755*.

Heffernan, J. E. and Tawn, J. A. (2001). Extreme value analysis of a large designed experiment: a case study in bulk carrier safety. *Extremes*, 4:359–378.

Jóhannesson, A. V., Siegert, S., Huser, R., Bakka, H., and Hrafnkelsson, B. (2022). Approximate Bayesian inference for analysis of spatiotemporal flood frequency data. *Annals of Applied Statistics*, 16(2):905–935.

Kingma, D. P. and Ba, J. (2014). Adam: A method for stochastic optimization. *arXiv preprint arXiv:1412.6980*.

Koh, J. (2023). Gradient boosting with extreme-value theory for wildfire prediction. *Extremes*, 26(2):273–299.

Krakauer, N. Y. (2024). Extending the blended generalized extreme value distribution. *Discover Civil Engineering*, 1(1):97.

Lawler, E. S. and Shaby, B. A. (2024). Anthropogenic and meteorological effects on the counts and sizes of moderate and extreme wildfires. *Environmetrics*, 35(7):e2873.

MacDonald, A., Scarrott, C. J., Lee, D., Darlow, B., Reale, M., and Russell, G. (2011). A flexible extreme value mixture model. *Computational Statistics & Data Analysis*, 55(6):2137–2157.

Mackay, E., Murphy-Barltrop, C., Richards, J., and Jonathan, P. (2024). Deep learning joint extremes of metocean variables using the SPAR model. *arXiv preprint arXiv:2412.15808*.

Majumder, R., Fang, S., Sankarasubramanian, A., Hector, E. C., and Reich, B. J. (2024a). Spatiotemporal density correction of multivariate global climate model projections using deep learning. *arXiv:2411.18799*.

Majumder, R. and Reich, B. J. (2023). A deep learning synthetic likelihood approximation of a non-stationary spatial model for extreme streamflow forecasting. *Spatial Statistics*, 55:100755.

Majumder, R., Reich, B. J., and Shaby, B. A. (2024b). Modeling extremal streamflow using deep learning approximations and a flexible spatial process. *The Annals of Applied Statistics*, 18(2):1519–1542.

McMahon, G., Gregonix, S. M., Waltman, S. W., Omernik, J. M., Thorson, T. D., Freeouf, J. A., Rorick, A. H., and Keys, J. E. (2001). Developing a spatial framework of common ecological regions for the conterminous United States. *Environmental Management*, 28(3):293–316.

Murphy, C., Tawn, J. A., and Varty, Z. (2024). Automated threshold selection and associated inference uncertainty for univariate extremes. *Technometrics*. To appear.

Nair, V. and Hinton, G. E. (2010). Rectified linear units improve restricted Boltzmann machines. In *Proceedings of the 27th International Conference on International Conference on Machine Learning*, ICML’10, page 807–814, Madison, WI, USA. Omnipress.

Naveau, P., Huser, R., Ribereau, P., and Hannart, A. (2016). Modeling jointly low, moderate, and heavy rainfall intensities without a threshold selection. *Water Resources Research*, 52(4):2753–2769.

Omernik, J. M. and Griffith, G. E. (2014). Ecoregions of the conterminous united states: Evolution of a hierarchical spatial framework. *Environmental Management*, 54(6):1249–1266.

Papastathopoulos, I. and Tawn, J. A. (2013). Extended generalised Pareto models for tail estimation. *Journal of Statistical Planning and Inference*, 143(1):131–143.

Pasche, O. C. and Engelke, S. (2024). Neural networks for extreme quantile regression with an application to forecasting of flood risk. *The Annals of Applied Statistics*, 18(4):2818–2839.

Prautzsch, H., Boehm, W., and Paluszny, M. (2002). *Bezier and B-Spline Techniques*. Springer-Verlag, Berlin, Heidelberg.

Prechelt, L. (2002). Early stopping-but when? In *Neural Networks: Tricks of the Trade*, pages 55–69. Springer.

Ramsay, J. O. (1988). Monotone regression splines in action. *Statistical Science*, pages 425–441.

Reynkens, T., Verbelen, R., Beirlant, J., and Antonio, K. (2017). Modelling censored losses using splicing: A global fit strategy with mixed Erlang and extreme value distributions. *Insurance: Mathematics and Economics*, 77:65–77.

Richards, J. (2022). pinnEV: Partially-Interpretable Neural Networks for modelling of Extreme Values. R package. Available at <https://github.com/Jbrich95/pinnEV>.

Richards, J. and Huser, R. (2022). Regression modelling of spatiotemporal extreme US wildfires via partially-interpretable neural networks. *arXiv preprint arXiv:2208.07581*.

Richards, J. and Huser, R. (2024). Extreme quantile regression with deep learning. In de Carvalho, M., Huser, R., Naveau, P., and Reich, B. J., editors, *Handbook on Statistics of Extremes*. Chapman & Hall/CRC.

Richards, J., Huser, R., Bevacqua, E., and Zscheischler, J. (2023). Insights into the drivers and spatio-temporal trends of extreme Mediterranean wildfires with statistical deep-learning. *Artificial Intelligence for the Earth Systems*, 2(4):e220095.

Scarrott, C. and MacDonald, A. (2012). A review of extreme value threshold estimation and uncertainty quantification. *REVSTAT-Statistical journal*, 10(1):33–60.

Stein, M. L. (2021a). A parametric model for distributions with flexible behavior in both tails. *Environmetrics*, 32(2):e2658.

Stein, M. L. (2021b). Parametric models for distributions when interest is in extremes with an application to daily temperature. *Extremes*, 24(2):293–323.

Tancredi, A., Anderson, C., and O'Hagan, A. (2006). Accounting for threshold uncertainty in extreme value estimation. *Extremes*, 9(2):87–106.

Tencaliec, P., Favre, A.-C., Naveau, P., Prieur, C., and Nicolet, G. (2020). Flexible semiparametric generalized Pareto modeling of the entire range of rainfall amount. *Environmetrics*, 31(2):e2582.

Velthoen, J., Cai, J.-J., Jongbloed, G., and Schmeits, M. (2019). Improving precipitation forecasts using extreme quantile regression. *Extremes*, 22:599–622.

Velthoen, J., Dombry, C., Cai, J.-J., and Engelke, S. (2023). Gradient boosting for extreme quantile regression. *Extremes*, 26(4):639–667.

Wang, H. J., Li, D., and He, X. (2012). Estimation of high conditional quantiles for heavy-tailed distributions. *Journal of the American Statistical Association*, 107(500):1453–1464.

Wilson, T., Tan, P.-N., and Luo, L. (2022). DeepGPD: A deep learning approach for modeling geospatial-temporal extreme events. *Proceedings of the AAAI Conference on Artificial Intelligence*, 36(4):4245–4253.

Xu, S. G. and Reich, B. J. (2021). Bayesian nonparametric quantile process regression and estimation of marginal quantile effects. *Biometrics*, 79:151–164.

Yadav, R., Huser, R., Opitz, T., and Lombardo, L. (2023). Joint modelling of landslide counts and sizes using spatial marked point processes with sub-asymptotic mark distributions. *Journal of the Royal Statistical Society Series C: Applied Statistics*, 72(5):1139–1161.

Youngman, B. D. (2019). Generalized additive models for exceedances of high thresholds with an application to return level estimation for US wind gusts. *Journal of the American Statistical Association*, 114(528):1865–1879.